RSC Advances

PAPER

View Article Online
View Journal | View Issue

Cite this: *RSC Adv.*, 2021, **11**, 20651

Design, synthesis and biological evaluation of 1*H*-pyrrolo[2,3-*b*]pyridine derivatives as potent fibroblast growth factor receptor inhibitors†

Xingping Su,‡[a] Zhihao Liu,‡[a] Lin Yue,[a] Xiuli Wu,[a] Wei Wei,[a] Hanyun Que,[a] Tinghong Ye,[a] Yi Luo*[b] and Yiwen Zhang*[a]

Received 5th April 2021
Accepted 18th May 2021

DOI: 10.1039/d1ra02660g

rsc.li/rsc-advances

Abnormal activation of FGFR signaling pathway plays an essential role in various types of tumors. Therefore, targeting FGFRs represents an attractive strategy for cancer therapy. Herein, we report a series of 1*H*-pyrrolo[2,3-*b*]pyridine derivatives with potent activities against FGFR1, 2, and 3. Among them, compound **4h** exhibited potent FGFR inhibitory activity (FGFR1–4 IC_{50} values of 7, 9, 25 and 712 nM, respectively). *In vitro*, **4h** inhibited breast cancer 4T1 cell proliferation and induced its apoptosis. In addition, **4h** also significantly inhibited the migration and invasion of 4T1 cells. Furthermore, **4h** with low molecular weight would be an appealing lead compound which was beneficial to the subsequent optimization. In general, this research has been developing a class of 1*H*-pyrrolo[2,3-*b*]pyridine derivatives targeting FGFR with development prospects.

1. Introduction

The fibroblast growth factor receptor (FGFR) family has four distinct isoforms (FGFR1–4) found across various tissue types and expressed to different extents under varying conditions.[1,2] The FGFR1–4 isoforms mainly consist of highly conserved extracellular ligand-binding domains, a single transmembrane segment, and a cytoplasmic tyrosine kinase domain.[3–5] Physiologically, the FGF–FGFR axis is involved in signal transduction pathways that regulate organ development, cell proliferation and migration, angiogenesis, and other processes.[6,7] Upon binding to fibroblast growth factors, the receptor undergoes dimerization and autophosphorylation of tyrosine residues in the cytoplasmic tail, resulting in activation of downstream signaling including RAS–MEK–ERK, PLCγ, and PI3K–Akt.[8,9]

Abnormal activation of FGFR signaling pathway due to amplification, fusion or missense mutations in the exon of FGFR family members is associated with the progression and development of several cancers such as breast cancer, lung cancer, prostate cancer, bladder cancer and liver cancer.[10–14] Moreover, activation of FGFR-dependent signaling pathways can facilitate cancer initiation, progression, and resistance to cancer therapy. Hence, the FGFR signaling pathway is an important and proven target for cancer therapeutics. Currently, FGFR inhibitors are currently under clinical investigation for the treatment of various cancers such as **AZD4547**,[15] **JNJ-42756493** (Erdafitinib),[16] **CH5183184**,[17] **BGJ-398**,[18] **LY2874455**,[19] **INCB054828** (Pemigatinib)[20] and so on, shown in Fig. 1. Recently, FDA has announced approval of Erdafitinib[21] and Pemigatinib.[22]

During the development of our FGFR inhibitor program, we wish to explore a novel and concise scaffold of selective FGFR inhibitors. Based on previous literature studies, we found that compound **1** has potent FGFR1 inhibitory activity with IC_{50} value of 1.9 μM (ref. 23) (Fig. 2A). Compared with the existing FGFR inhibitors, compound **1** contains a novel core scaffold 1*H*-pyrrolo[2,3-*b*]pyridine with low molecular mass and high ligand efficiency. Jin Q. *et al.* developed a series of 1*H*-pyrrolo[2,3-*b*]pyridine derivatives as FGFR4 inhibitors with potent anti-proliferative activity against Hep3B cells.[24] Furthermore, 1*H*-pyrrolo[2,3-*b*]pyridine also as a new scaffold used in other targets research, such as human neutrophil elastase (HNE).[25] Moreover, recent studies have shown that 1*H*-pyrrolo[2,3-*b*]pyridine analogues have inhibitory activity against different cancer cell lines.[26]

We firstly investigated the co-crystallization structure (PDB code 3C4F) to understand interactions between **1** and FGFR1 kinase domain (Fig. 2B). As a hinge binder, 1*H*-pyrrolo[2,3-*b*]pyridine ring of **1** could form two hydrogen bonds with the backbone carbonyl of E562 and NH of A564 in the hinge region. The methoxyphenyl motif could potentially occupy hydrophobic pocket in the ATP site and form van der Waals interactions with amino acid residues of the hydrophobic pocket, and its methoxy

[a]*Sichuan University-University of Oxford Huaxi Joint Centre for Gastrointestinal Cancer, State Key Laboratory of Biotherapy, West China Hospital, Sichuan University, Chengdu, Sichuan, 610041, China. E-mail: yiwenzhang@scu.edu.cn*

[b]*Department of Orthopedics, West China Hospital of Sichuan University, Wai Nan Guo Xue Xiang 37#, 610041, Chengdu, Sichuan, China. E-mail: orthop_luoyi@163.com*

† Electronic supplementary information (ESI) available. See DOI: 10.1039/d1ra02660g

‡ These authors contributed equally to this work.

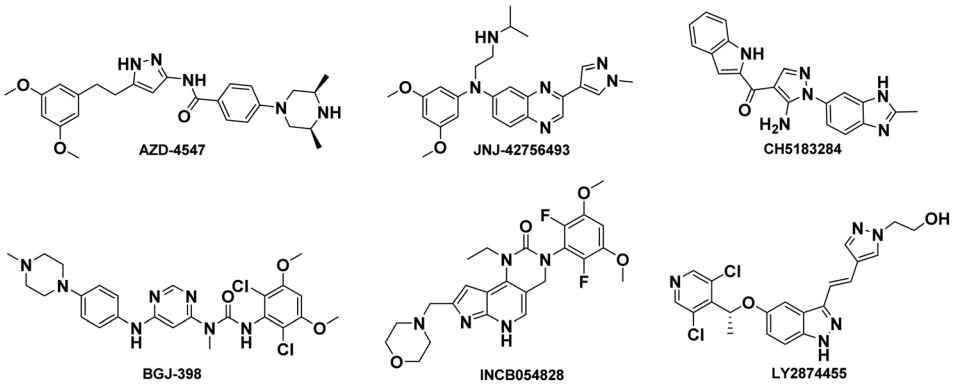

Fig. 1 Chemical structure of representative FGFR inhibitors.

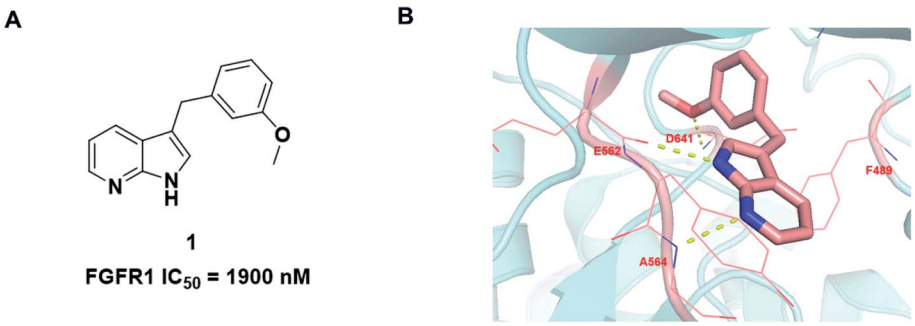

Fig. 2 (A) Chemical structure of compound **1**. (B) The binding mode of **1** with FGFR1.

group could also form a strong hydrogen bond with the NH of D641.

Based on above analyses, to quest for a novel and concise chemotype of FGFR inhibitors, we kept 1*H*-pyrrolo[2,3-*b*]pyridine motif as hinge binder and focused on utilizing structure-based design strategy to design 1*H*-pyrrolo[2,3-*b*]pyridine derivatives as potent FGFR inhibitors. Given that the 5-position of 1*H*-pyrrolo[2,3-*b*]pyridine is close to G485, a group which could provide hydrogen bond acceptor with suitable size was introduced into the 5-position of 1*H*-pyrrolo[2,3-*b*]pyridine ring to form a hydrogen bond with G485 to improve the activity. Meanwhile, the *m*-methoxyphenyl fragment was altered to various larger substituents to explore the possible interactions within the hydrophobic pocket. In this study, we report the synthesis and biology evaluation of 1*H*-pyrrolo[2,3-*b*]pyridine derivatives as potent FGFR inhibitors.

The synthesis of all compounds is shown in Scheme 1. The starting material 5-(trifluoromethyl)-1*H*-pyrrolo[2,3-*b*]pyridine was reacted with *R*-substituted aldehyde at 50 °C to obtain the compounds **3a–3k** in 45–60% yield. Subsequently, **3a–3k** in the presence of acetonitrile under triethylsilane and trifluoroacetic acid catalysis at reflux to undergo a reduction reaction to furnish **4a–4l** in 46–80%.

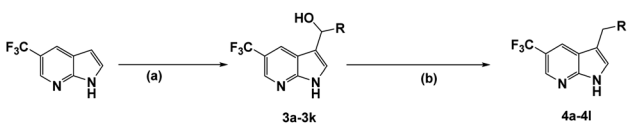

Scheme 1 [a]Synthesis of target compounds. [a]Reagents and conditions: (a) R–CHO, potassium hydroxide, methanol, 50 °C, 5 h, 45–60%; (b) triethylsilane, trifluoroacetic acid, acetonitrile, reflux, 2 h, 46–80%.

All prepared compounds were screened for their inhibitory activity against FGFR1 at the concentration of 0.1 and 1 μM as well as antiproliferative activities against 4T1 (mouse breast cancer cells), MDA-MB-231 and MCF-7 cancer cells at 10 μM. As summarized in Tables 1 and 2, compound **1** with low molecular mass demonstrated FGFR1 potency with an IC_{50} value of 1900 nM. Based on our analysis above, a suitably sized trifluoromethyl was introduced at the 5-position of the 1*H*-pyrrolo [2,3-*b*]pyridine ring (**4a**) in **1** to form hydrogen bond with G485. Remarkably, the activity against FGFR1 of **4a** increased nearly 20-fold compared with compound **1**, implying that our strategy was feasible. Then the *m*-methoxy moiety of **4a** was modified to improve FGFR activities. The methoxy group at the 3-position of phenyl ring in **4a** replaced with chlorine (**4b**) decreased FGFR1 potency and cellular activity. Poor activities of **4b** may be due to the weak electronegativity of Cl atom in **4b** which cannot form strong hydrogen bond with D641. Introduction of 3-trifluoromethyl group at the 3-position of phenyl ring reduced the activities of **4c**, which may be result from the inability of trifluoromethyl group to form a hydrogen bond with the NH of D641. The introduction of suitable group at the 3-position of phenyl ring to occupy the hydrophobic pocket improved the

Table 1 Biological results of **3a–3k**[a]

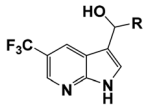

Compound	R	FGFR1 inhibition rate (%)		Inhibition rate 10 μM (%)		
		1 μM	0.1 μM	4T1	MDA-MB-231	MCF-7
1	—	55	7	11 ± 0.02	8 ± 2.14	16 ± 0.62
3a	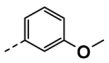	78	35	16 ± 0.01	6 ± 1.22	33 ± 0.50
3b	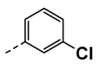	25	1	NS	10 ± 2.88	14 ± 3.18
3c	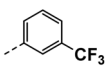	22	22	NS	23 ± 0.63	33 ± 0.71
3d	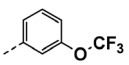	22	−5	NS	12 ± 1.50	21 ± 0.82
3e	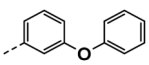	34	15	NS	NS	26 ± 0.88
3f	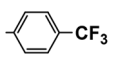	25	14	NS	18 ± 0.70	33 ± 1.10
3g	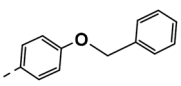	25	−1	NS	28 ± 0.23	25 ± 1.05
3h	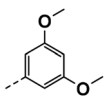	89	61	23 ± 0.01	13 ± 3.80	33 ± 0.11
3i	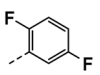	61	19	NS	21 ± 1.87	32 ± 1.24
3j	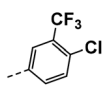	17	3	NS	15 ± 0.97	30 ± 1.17
3k	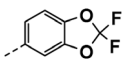	11	3	NT	NT	NT

[a] Cell results are given in concentrations of 10 μM after a continuous exposure of 72 h and show means ± SD of two-independent experiments. NS: not significant; NT: not tested.

FGFR1 activity (**4a–e**), indicating a suitable size of the group on this position was favorable. Incorporation of a trifluoromethyl (**4f**) or benzyloxy (**4g**) at the 4-position of phenyl ring declined both FGFR1 and cellular activities. Then the influence of substituents on 3- and 5-positions of the phenyl ring **4a** was investigated. Excitingly, introduction of methoxy groups at the 3- and 5-positions significantly improved against FGFR1 potency (**4h**) (95% & 0.1 μM) and cellular activity (4T1) (57% & 10 μM). However, multiple substitutions at other positions (**4i**, **4j**, **4k**, **4l**) exhibited declined FGFR1 and cellular activities. In addition, the presence of a hydroxyl also decreased FGFR1 potency and cellular activity (**4a** *vs.* **3a**), (**4h** *vs.* **3h**) which implicated that the hydroxyl group may be too close to its neighboring amino acid F489, resulting in decreased activities.

Compound **3h**, **4a**, **4h** and **4l** were selected to investigate their inhibitory activities against other FGFR isoforms, including FGFR1, FGFR2, FGFR3 and FGFR4 (Table 3). All these compounds exhibited inhibitory activities to FGFR1–3 *in vitro*. Among them, **4h** showed the best activities that effectively inhibited the activities of FGFR1–4 with IC_{50} values of 7, 9, 25 and 712 nM, respectively. Based on above results, **4h** was chosen for further biological evaluation.

To investigate the binding modes of our inhibitors, compound **4h** was docked with FGFR1 protein, as showed in Fig. 3. The nucleus 1*H*-pyrrolo[2,3-*b*]pyridine could form two hydrogen bonds with the backbone carbonyl of E562 and NH of A564 in the hinge region. In addition, the essential π–π interaction was observed between 3,5-dimethoxyphenyl of **4h** and

Table 2 Biological results of 4a–4l[a]

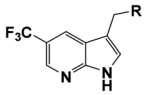

Compound	R	FGFR1 inhibition rate (%)		Inhibition rate 10 μM (%)		
		1 μM	0.1 μM	4T1	MDA-MB-231	MCF-7
4a	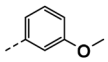	91	53	18 ± 0.01	15 ± 1.16	32 ± 0.54
4b	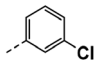	56	2	NS	6.1 ± 0.16	29 ± 0.83
4c	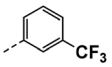	19	10	26 ± 0.04	29 ± 0.24	51 ± 0.17
4d	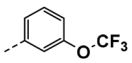	21	15	NS	25 ± 0.36	27 ± 3.33
4e	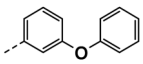	64	21	NS	16 ± 0.54	26 ± 1.65
4f	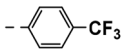	21	24	17 ± 0.02	20 ± 2.60	44 ± 0.73
4g	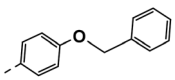	29	−4	NS	25 ± 2.44	32 ± 0.24
4h	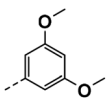	91	95	57 ± 0.01	22 ± 0.08	33 ± 0.94
4i	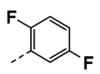	78	29	NS	14 ± 3.18	41 ± 0.71
4j	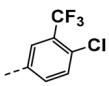	16	7	13 ± 0.02	19 ± 0.38	46 ± 1.09
4k	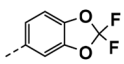	40	19	22 ± 0.03	20 ± 0.03	46 ± 0.49
4l	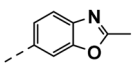	76	27	23 ± 0.01	9 ± 0.62	22 ± 1.66

[a] Cell results are given in concentrations of 10 μM after a continuous exposure of 72 h and show means ± SD of two-independent experiments. NS: not significant.

Table 3 FGFR selectivity of selected compounds

Compound	IC_{50} (nM)			
	FGFR1	FGFR2	FGFR3	FGFR4
3h	54	66	320	>3000
4a	83	93	421	>3000
4h	7	9	25	712
4l	266	259	634	>3000
AZD-4547	0.8	1	2	47

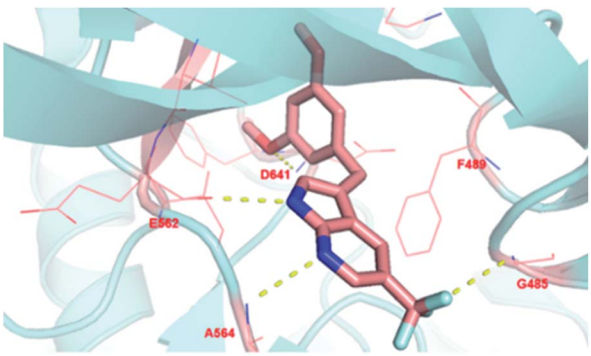

Fig. 3 Proposed binding mode of compound **4h** to FGFR1 kinase domain.

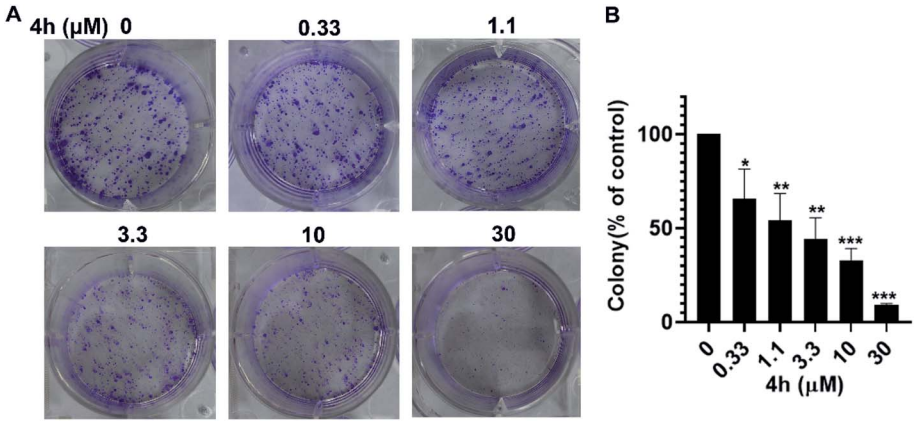

Fig. 4 **4h** inhibits the proliferation of 4T1 cells. (A) The effects of **4h** on colony formation in 4T1 cell for 8–12 days. (B) The statistical results of colony formation assays were presented as surviving colonies. Data are expressed as mean ± SD. From two-independent experiments (*p < 0.05, **p < 0.01 and ***p < 0.001).

F489. Then, the 3,5-dimethoxyphenyl group could more fully and appropriately occupy the hydrophobic pocket and maintain the formation of hydrogen bonds with D641. As expected, trifluoromethyl substitution at the 5-position of 1*H*-pyrrolo[2,3-*b*] pyridine could form a hydrogen bond with G485, which may be a crucial factor in improving the activity of the compound. In addition, the ligand efficiency of **4h** (LE = 0.44) has been significantly improved compared with compound **1** (LE = 0.13).

To further investigate whether **4h** could inhibit the proliferation of 4T1 cells, we conducted the colony formation assays. As showed in Fig. 4, the colony formation of 4T1 cells was reduced after treatment with **4h**. Moreover, **4h** could inhibit the population-dependence growth of 4T1 cells. These results suggest that **4h** could inhibit 4T1 cells viability in a concentration-dependent manner.

To quantify whether the anti-survival activity of **4h** in 4T1 cells was related to apoptosis. We analyzed the level of apoptosis

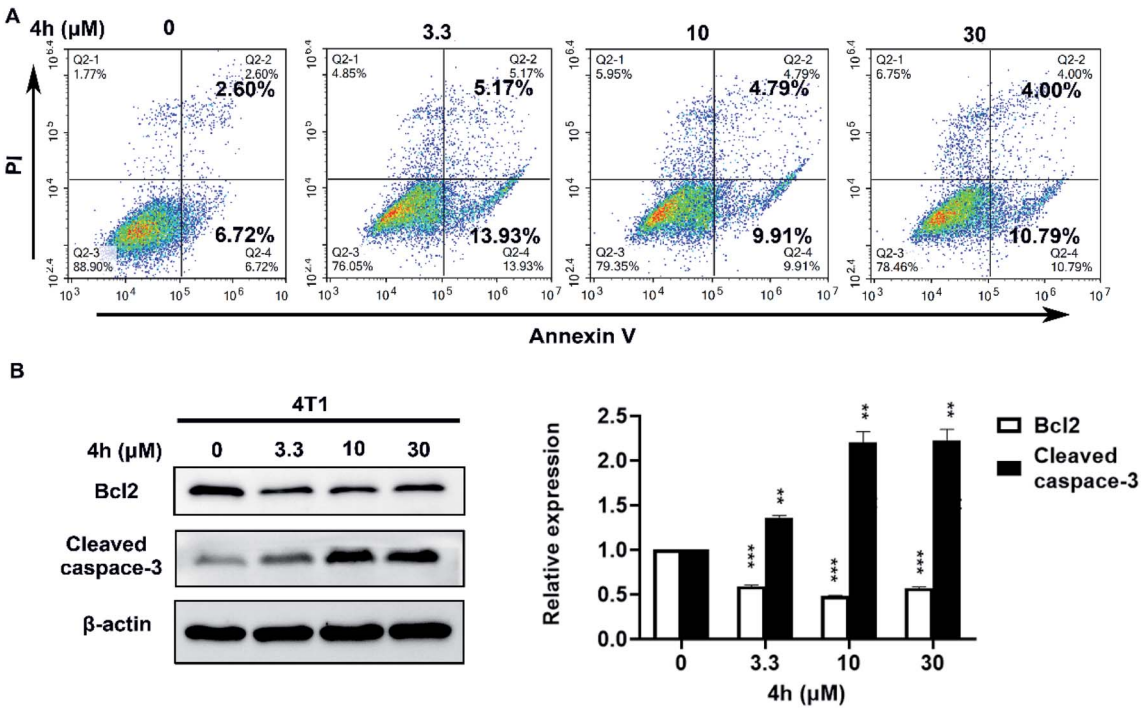

Fig. 5 **4h** induces 4T1 cell apoptosis. (A) 4T1 cells were exposed to **4h** at indicated doses for 24 h. Annexin V/PI double labeling technology detects the level of cell apoptosis, and the flow cytometer detects the level of cell apoptosis. (B) Western blot analyses of 4T1 cells treated with different concentrations of **4h** for 24 h to evaluate protein expression of Bcl2 and cleaved caspase-3. The protein expression was quantified by densitometry analysis using Image-Pro Plus. Data are expressed as mean ± SD from two-independent experiments (**p < 0.01, ***p < 0.001, compared to control).

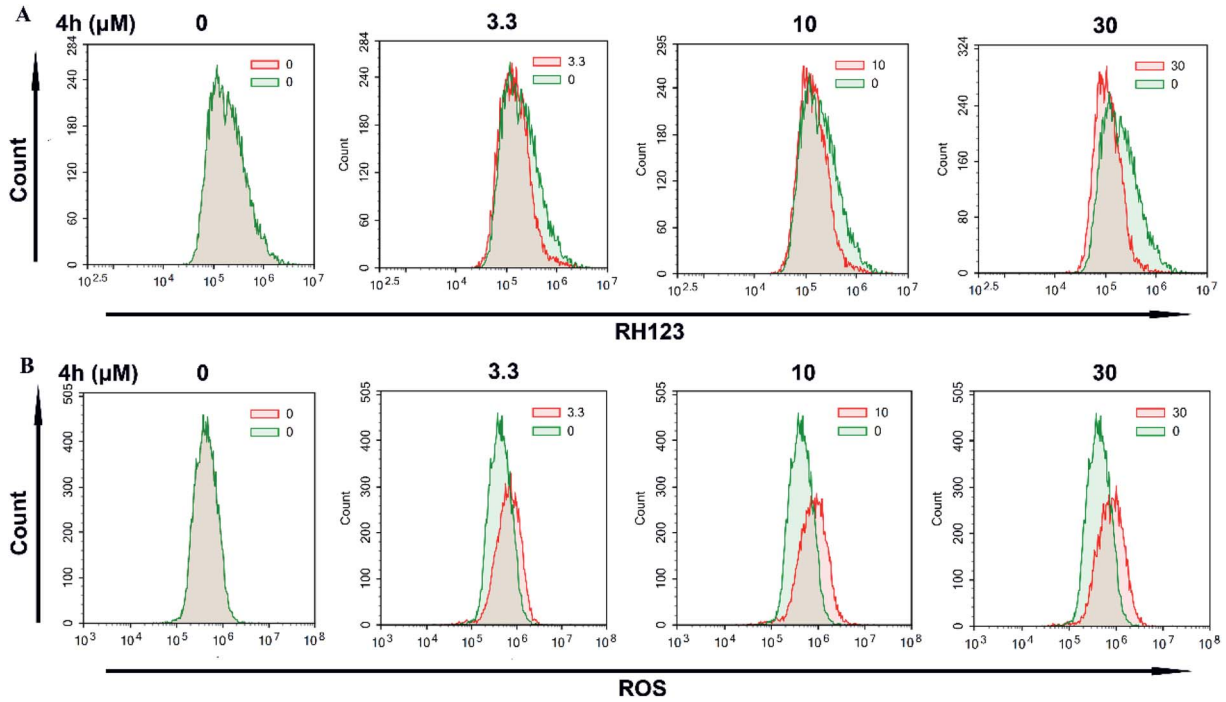

Fig. 6 Changes in mitochondrial membrane potential and accumulation of ROS. (A) 4T1 cells were treated with different concentrations of **4h** for 24 h. (B) 4T1 cells were treated with **4h** at indicated doses for 24 h, and then ROS levels were analyzed with a flow cytometer.

by FCM using the Annexin V–FITC/PI double labelling technique. As Fig. 5A indicated, the **4h** could induce 4T1 cells apoptosis compared with vehicle after treatment with **4h** for 24 h. Then we performed western blot analysis to further characterize **4h**-induced apoptosis (Fig. 5B). The expression level of anti-apoptotic protein Bcl2 was decreased, whereas the proapoptotic protein cleaved caspase-3 was increased in a dose-dependent manner after **4h** treatment in 4T1 cells. These data suggest that **4h** could induce 4T1 cell apoptosis.

Next, we used FCM to detect the change of $\Delta\psi_m$ after staining with the fluorescent dye Rh123. As showed in Fig. 6A, treatment with **4h** for 24 h resulted in a loss of $\Delta\psi_m$ in 4T1 cells. Furthermore, we examined the ROS level by FCM using the DCFH-DA indicator (Fig. 6B). The results showed that the level of ROS in 4T1 cells increased after treatment with **4h** for 24 h. These data indicated that **4h** was able to induce apoptosis of 4T1 cell, and it might be *via* the mitochondrial apoptosis pathway.

Furthermore, we evaluated the effect of compound **4h** on the migration and invasion abilities of 4T1 cells through the transwell chamber assay. As showed in Fig. 7, **4h** significantly reduced the migration and invasion abilities of 4T1 cells after treatment of **4h** for 24 h. Compared to the control group, 4T1 cells migration was inhibited by 36.1%, 77.3%, and 93.8% following treatment with 3.3, 10 and 30 μM **4h**, respectively (Fig. 7A). Similarly, 4T1 cells also exhibited significantly decreased invasion in the presence of **4h** compared to control group (Fig. 7B). Furthermore, we detected the expression level of several key proteins by western blot. After **4h** interfered with 4T1 cells for 24 h, the expression of MMP9 decreased with the increase of **4h** concentration, while the expression of TIMP2 gradually increased (Fig. 7C). The results implied that **4h** could enhance inhibition of migration and invasion of 4T1 cells which associated with down-regulation of MMP9 and up-regulation of TIMP2.

In conclusion, we discovered a series of 1*H*-pyrrolo[2,3-*b*] pyridine derivatives as potent FGFR inhibitors. Structure optimization of **1** led to the identification of **4h**, which had pan-FGFR inhibitory activities against FGFR1–4 (IC_{50} values of 7, 9, 25 and 712 nM, respectively) and nearly 300-fold higher FGFR1 activity than compound **1**, showing a highly ligand efficiency (ligand efficiency increased from 0.13 to 0.44). Accordingly, we selected compound **4h** for further biological activity evaluation, and the results showed that **4h** could inhibit proliferation, induce apoptosis, and significantly inhibit the migration and invasion of 4T1 cells. These data indicated that low molecular weight **4h** would be a promising lead compound with a large optimization space for further drug development.

2. Experimental section

2.1. Chemistry

All reagents and chemicals used in this study do not require further purification and are commercially available. TLC was performed on 0.20 mm silica gel 60 F254 plates (Qingdao Ocean Chemical Factory, Shandong, China). Visualization of spots on TLC plates were done by UV light and I_2. ^1H (400 MHz) and ^{13}C (101 MHz) NMR spectra were recorded on Bruker Avance 400 spectrometer (Bruker Company, Germany) with $CDCl_3$, DMSO-d_6 or CD_3OD as solvent and TMS as an internal standard. All

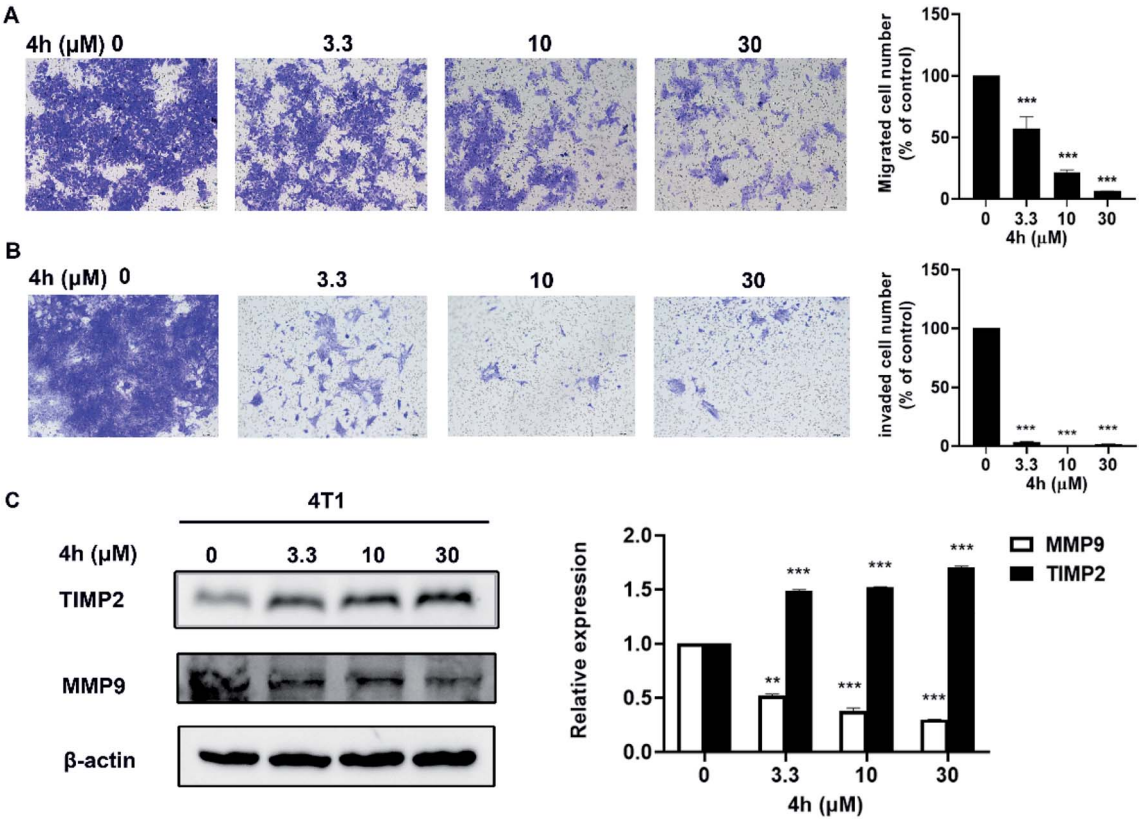

Fig. 7 Inhibition of migratory and invasive in 4T1 cells by **4h** treated. (A) 4T1 cells were seeded in the top chamber of transwell with serum-free medium, without Matrigel in the upper chamber, treated with vehicle or various concentrations of **4h**. After about 24 h, migrated cells were fixed, stained, photographed (10×) and quantified. (B) 4T1 cell were treated with different concentrations of **4h** and allowed to invade through Matrigel for 24 h. Invaded cell numbers were counted (10×). (C) Western blot analyses of 4T1 cells treated (24 h) with different concentrations of **4h** were used to evaluate protein expression of MMP9 and TIMP2. β-Actin served as loading control. Data are expressed as mean ± SD from two-independent experiments (**$p < 0.01$, ***$p < 0.001$, compared to control).

chemical shift values were reported in units of δ (ppm). The following abbreviations were used to indicate the peak multiplicity: s = singlet; d = doublet; t = triplet; q = quart; m = multiplet; high-resolution mass data (MS) were obtained by Q-TOF Premier mass spectrometer (Micromass, Manchester, UK).

2.1.1 General procedure for the synthesis of 3a–3k. To 5-(trifluoromethyl)-1*H*-pyrrolo[2,3-*b*]pyridine (187 mg, 1 mmol) in methanol (7 mL) were added *m*-dimethoxybenzaldehyde (150 mg, 1.1 mmol), and potassium hydroxide (281 mg, 5 mmol). The reaction was stirred at 50 °C for 5 hours. The reaction was poured into water, and extracted with ethyl acetate. The organic layer was dried over anhydrous sodium sulfate, and filtered. The filtrate was concentrated and purified by column chromatography using silica with 5% MeOH in DCM as the eluent to give **3a** (180 mg, 56% yield), as a white solid. ^{1}H NMR (400 MHz, DMSO-d_6) δ 12.01 (s, 1H), 8.54 (d, J = 2.1 Hz, 1H), 8.27 (d, J = 2.2 Hz, 1H), 7.55 (d, J = 2.0 Hz, 1H), 7.20 (t, J = 7.8 Hz, 1H), 6.97–6.87 (m, 2H), 6.79–6.71 (m, 1H), 4.10 (s, 2H), 3.72 (s, 3H). ^{13}C NMR (101 MHz, DMSO-d_6) δ 159.78, 150.37, 143.01, 139.59, 129.81, 127.07, 126.77, 124.79 (d, J = 3.9 Hz), 124.38, 121.16, 118.70, 117.08 (q, J = 31.3 Hz), 114.74, 111.69, 55.36, 31.06. HRMS *m*/*z* (ESI) calcd for $C_{17}H_{15}N_2O_3F_3Na$ $[M + Na]^+$: 345.0821, found: 345.0539.

3b: ^{1}H NMR (400 MHz, DMSO-d_6) δ 12.04 (s, 1H), 8.53 (d, J = 2.2 Hz, 1H), 8.18 (d, J = 2.2 Hz, 1H), 7.55–7.42 (m, 3H), 7.42–7.34 (m, 2H), 6.04 (d, J = 4.6 Hz, 1H), 5.96 (d, J = 4.6 Hz, 1H). ^{13}C NMR (101 MHz, DMSO-d_6) δ 150.52, 144.45, 139.79, 139.75, 131.73, 128.51, 128.47, 126.21, 125.55, 125.51, 119.74, 117.88–116.60 (m), 117.27, 68.15. HRMS *m*/*z* (ESI) calcd for $C_{15}H_{11}N_2OF_3Cl$ $[M + H]^+$: 327.0507, found: 327.0513.

3c: ^{1}H NMR (400 MHz, DMSO-d_6) δ 12.07 (s, 1H), 8.53 (d, J = 2.4 Hz, 1H), 8.19 (d, J = 2.2 Hz, 1H), 7.87 (s, 1H), 7.74 (d, J = 7.4 Hz, 1H), 7.63–7.53 (m, 2H), 7.50 (d, J = 1.8 Hz, 1H), 6.15 (d, J = 4.6 Hz, 1H), 6.10 (d, J = 4.6 Hz, 1H); ^{13}C NMR (101 MHz, DMSO-d_6) δ 150.51, 146.94, 139.80, 130.80, 129.55 (d, J = 19.5 Hz), 130.17–128.56 (m), 126.93, 126.35, 125.46 (d, J = 3.9 Hz), 124.01 (d, J = 4.0 Hz), 122.94 (d, J = 3.9 Hz), 119.44, 117.26 (q, J = 31.3 Hz), 117.18, 68.16. HRMS *m*/*z* (ESI) calcd for $C_{16}H_{11}N_2OF_6$ $[M + H]^+$: 361.0770, found: 361.0770.

3d: ^{1}H NMR (400 MHz, chloroform-*d*) δ 9.83 (s, 1H), 8.57 (d, J = 2.1 Hz, 1H), 8.16 (d, J = 2.0 Hz, 1H), 7.47–7.36 (m, 3H), 7.24–7.15 (m, 2H), 6.20–6.15 (m, 1H); ^{13}C NMR (101 MHz, chloroform-*d*) δ 150.10, 149.53, 145.00, 140.68, 130.04, 126.17, 125.91, 125.00, 124.73, 123.22, 120.37, 118.98, 118.67, 117.46, 69.63, 29.71. HRMS *m*/*z* (ESI) calcd for $C_{16}H_{11}N_2O_2F_6$ $[M + H]^+$: 377.0719, found: 377.0684.

3e: ^{1}H NMR (400 MHz, DMSO-d_6) δ 12.10–11.96 (m, 1H), 8.53 (d, J = 2.1 Hz, 1H), 8.10 (d, J = 2.2 Hz, 1H), 7.48 (d, J = 2.4 Hz, 1H), 7.35 (m, J = 7.9, 6.2, 3.4 Hz, 3H), 7.25–7.18 (m, 1H), 7.17–7.08 (m, 2H), 7.01–6.93 (m, 2H), 6.89 (m, J = 8.1, 2.6, 1.1 Hz, 1H), 6.01 (d, J = 4.6 Hz, 1H), 5.91 (d, J = 4.6 Hz, 1H). ^{13}C NMR (101 MHz, DMSO-d_6) δ 157.21, 156.94, 150.52, 147.86, 139.72, 139.68, 130.39, 130.16, 126.98, 126.27, 125.52 (d, J = 3.8 Hz), 124.28, 123.79, 121.94, 119.79, 118.88, 117.81–116.51 (m), 68.44. HRMS m/z (ESI) calcd for $C_{21}H_{16}N_2O_2F_3$ $[M + H]^+$: 385.1158, found: 385.1156.

3f: ^{1}H NMR (400 MHz, DMSO-d_6) δ 12.08 (s, 1H), 8.53 (d, J = 2.2 Hz, 1H), 8.20 (d, J = 2.3 Hz, 1H), 7.70 (s, 4H), 7.50 (d, J = 2.4 Hz, 1H), 6.23–6.03 (m, 2H). ^{13}C NMR (101 MHz, DMSO-d_6) δ 162.75, 150.49, 150.15, 139.81, 128.08, 127.77, 127.32, 126.95, 126.40, 126.16, 125.47, 124.25, 123.46, 119.38, 117.27 (q, J = 31.5 Hz), 68.26. HRMS m/z (ESI) calcd for $C_{16}H_{11}N_2OF_6$ $[M + H]^+$: 361.0770, found: 361.0767.

3g: ^{1}H NMR (400 MHz, methanol-d_4) δ 8.45 (d, J = 2.1 Hz, 1H), 8.13 (d, J = 2.3 Hz, 1H), 7.40–7.32 (m, 2H), 7.33–7.21 (m, 6H), 7.10 (t, J = 2.1 Hz, 1H), 7.06 (dt, J = 8.1, 1.0 Hz, 1H), 7.02–6.87 (m, 2H), 6.05 (s, 1H), 5.07 (s, 2H). ^{13}C NMR (101 MHz, DMSO-d_6) δ 158.08, 149.06, 144.43, 138.33, 136.45, 128.21, 127.19, 126.56, 126.24, 124.94, 124.86, 118.24, 118.03, 117.29–116.69 (m), 113.08, 112.04, 68.73, 68.49. HRMS m/z (ESI) calcd for $C_{22}H_{18}N_2O_2F_3$ $[M + H]^+$: 399.1315, found: 399.1305.

3h: ^{1}H NMR (400 MHz, DMSO-d_6) δ 12.04 (s, 1H), 8.53 (d, J = 2.2 Hz, 1H), 8.18 (d, J = 2.2 Hz, 1H), 7.55–7.42 (m, 3H), 7.42–7.34 (m, 2H), 6.04 (d, J = 4.6 Hz, 1H), 5.96 (d, J = 4.6 Hz, 1H). ^{13}C NMR (101 MHz, DMSO-d_6) δ 150.52, 144.45, 139.79, 139.75, 131.73, 128.93, 128.73, 128.51, 128.47, 126.21, 125.55, 125.51, 119.74, 117.34, 117.27, 117.03, 68.15. HRMS m/z (ESI) calcd for $C_{17}H_{16}N_2O_3F_3$ $[M + H]^+$: 353.1108, found: 353.1108.

3i: ^{1}H NMR (400 MHz, DMSO-d_6) δ 12.10 (s, 1H), 8.55 (d, J = 2.2 Hz, 1H), 8.28 (d, J = 2.2 Hz, 1H), 7.49 (dd, J = 6.2, 3.1 Hz, 1H), 7.39 (d, J = 2.5 Hz, 1H), 7.26–7.07 (m, 2H), 6.24 (d, J = 4.9 Hz, 1H), 6.11 (dd, J = 5.0, 1.8 Hz, 1H). ^{13}C NMR (101 MHz, DMSO-d_6) δ 159.96, 157.59 (d, J = 2.0 Hz), 156.70 (d, J = 2.2 Hz), 154.30, 150.37, 139.87 (d, J = 3.8 Hz), 134.43 (dd, J = 16.1, 7.0 Hz), 126.42, 125.28 (d, J = 4.0 Hz), 124.27, 118.07, 117.30, 115.64 (d, J = 24.3 Hz), 114.52 (d, J = 20.2 Hz), 62.54. HRMS m/z (ESI) calcd for $C_{15}H_{10}N_2OF_5$ $[M + H]^+$: 329.0708, found: 329.2583.

3j: ^{1}H NMR (400 MHz, DMSO-d_6) δ 12.10 (s, 1H), 8.55 (d, J = 2.2 Hz, 1H), 8.25 (d, J = 2.2 Hz, 1H), 7.98 (d, J = 2.0 Hz, 1H), 7.75 (dd, J = 8.3, 2.1 Hz, 1H), 7.72–7.63 (m, 1H), 7.50 (d, J = 2.4 Hz, 1H), 6.26–6.09 (m, 2H). ^{13}C NMR (101 MHz, DMSO-d_6) δ 150.51, 145.57, 139.93, 139.89, 132.31, 131.93, 129.37, 129.35, 126.53, 125.75, 125.70, 125.48, 125.44, 119.06, 118.09–116.25 (m), 67.57. HRMS m/z (ESI) calcd for $C_{16}H_{10}N_2OF_6Cl$ $[M + H]^+$: 395.0380, found: 395.0367.

3k: ^{1}H NMR (400 MHz, DMSO-d_6) δ 12.06 (s, 1H), 8.53 (d, J = 2.1 Hz, 1H), 8.24 (d, J = 2.1 Hz, 1H), 7.56–7.41 (m, 2H), 7.39–7.27 (m, 2H), 6.05 (d, J = 10.5 Hz, 2H). ^{13}C NMR (101 MHz, chloroform-d) δ 150.14, 144.08, 143.37, 140.46, 139.05, 131.67, 129.13, 126.24, 125.06, 123.22, 121.63, 118.75, 117.58, 109.29, 108.00, 69.88. HRMS m/z (ESI) calcd for $C_{16}H_{10}N_2O_3F_5$ $[M + H]^+$: 373.0606, found: 373.0583.

2.1.2 General procedure for the synthesis of 4a–4l. To **3a** (100 mg, 0.31 mmol) in acetonitrile (7 mL) were added triethylsilane (1.00 mL, 6.26 mmol) and trifluoroacetic acid (0.50 mL, 6.54 mmol). The reaction was heated to reflux for 2 hours. The reaction was poured into aqueous potassium carbonate, and extracted with ethyl acetate. The organic layer was dried over anhydrous sodium sulfate, and filtered. The filtrate was concentrated and purified by column chromatography using silica with 5% MeOH in DCM as the eluent to give **4a** (57 mg, 60% yield), as a white solid. ^{1}H NMR (400 MHz, DMSO-d_6) δ 11.97 (s, 1H), 8.52 (d, J = 2.1 Hz, 1H), 8.25 (d, J = 2.1 Hz, 1H), 7.53 (d, J = 2.2 Hz, 1H), 7.19 (t, J = 7.8 Hz, 1H), 6.95–6.85 (m, 2H), 6.75 (dd, J = 8.2, 2.6 Hz, 1H), 4.08 (s, 2H), 3.71 (s, 3H). ^{13}C NMR (101 MHz, DMSO-d_6) δ 159.78, 150.37, 143.01, 139.56, 129.81, 126.78, 124.78, 121.16, 118.70, 117.08 (q, J = 31.3 Hz), 114.74, 114.65, 111.69, 55.37, 31.06. HRMS m/z (ESI) calcd for $C_{16}H_{14}N_2OF_3$ $[M + H]^+$: 307.1053, found: 307.1052.

4b: ^{1}H NMR (400 MHz, DMSO-d_6) δ 12.00 (s, 1H), 8.52 (d, J = 2.1 Hz, 1H), 8.24 (d, J = 2.2 Hz, 1H), 7.53 (d, J = 2.4 Hz, 1H), 7.33 (s, 4H), 4.13–4.09 (m, 2H). ^{13}C NMR (101 MHz, DMSO-d_6) δ 150.36, 140.50, 139.69, 139.65, 130.99, 130.72, 128.72, 126.95, 124.76, 124.72, 121.65, 118.60, 117.17 (q, J = 31.3 Hz), 114.30, 30.24. HRMS m/z (ESI) calcd for $C_{15}H_{11}N_2F_3Cl$ $[M + H]^+$: 311.0557, found: 311.0593.

4c: ^{1}H NMR (400 MHz, DMSO-d_6) δ 12.02 (s, 1H), 8.53 (d, J = 2.1 Hz, 1H), 8.30 (d, J = 2.1 Hz, 1H), 7.72 (s, 1H), 7.68–7.57 (m, 2H), 7.57–7.46 (m, 2H), 4.23 (s, 2H). ^{13}C NMR (101 MHz, DMSO-d_6) δ 150.35, 143.04, 139.69, 133.08, 129.85, 129.69, 129.38, 127.07, 125.37 (d, J = 3.9 Hz), 124.84 (d, J = 3.7 Hz), 123.16 (d, J = 4.1 Hz), 118.56, 117.80–116.16 (m), 114.00, 30.58. HRMS m/z (ESI) calcd for $C_{16}H_{11}N_2F_6$ $[M + H]^+$: 345.0821, found: 345.0833.

4d: ^{1}H NMR (400 MHz, DMSO-d_6) δ 12.01 (s, 1H), 8.52 (d, J = 2.1 Hz, 1H), 8.25 (d, J = 2.1 Hz, 1H), 7.59 (d, J = 2.4 Hz, 1H), 7.48–7.29 (m, 3H), 7.17 (d, J = 8.1 Hz, 1H), 4.18 (s, 2H). ^{13}C NMR (101 MHz, DMSO-d_6) δ 150.37, 148.90, 144.39, 139.65, 130.66, 128.08, 126.97, 124.84, 121.36, 118.88, 118.54, 117.21 (q, J = 31.5 Hz), 113.95, 55.34, 30.62. HRMS m/z (ESI) calcd for $C_{16}H_{11}N_2OF_6$ $[M + H]^+$: 361.0770, found: 361.0784.

4e: ^{1}H NMR (400 MHz, DMSO-d_6) δ 12.06–11.90 (m, 1H), 8.52 (d, J = 2.1 Hz, 1H), 8.19 (d, J = 2.1 Hz, 1H), 7.54 (d, J = 2.3 Hz, 1H), 7.38–7.25 (m, 3H), 7.14–7.06 (m, 2H), 7.03–6.89 (m, 3H), 6.81 (dd, J = 8.2, 2.4 Hz, 1H), 4.11 (s, 2H). ^{13}C NMR (101 MHz, DMSO-d_6) δ 157.17, 157.02, 150.36, 143.77, 139.63, 130.39, 127.04, 126.88, 124.74, 124.18, 123.72, 119.27, 118.78, 118.63, 117.13 (q, J = 31.3 Hz), 116.71, 114.33, 30.85. HRMS m/z (ESI) calcd for $C_{21}H_{16}N_2OF_3$ $[M + H]^+$: 369.1209, found: 369.1253.

4f: ^{1}H NMR (400 MHz, DMSO-d_6) δ 12.06 (s, 1H), 8.54 (d, J = 2.1 Hz, 1H), 8.36 (d, J = 2.1 Hz, 1H), 7.86 (s, 1H), 7.61 (dd, J = 6.8, 1.9 Hz, 3H), 4.22 (s, 2H). ^{13}C NMR (101 MHz, DMSO-d_6) δ 150.33, 146.47, 139.74, 129.64, 127.36, 127.16, 127.04, 126.21, 125.65, 124.75, 124.33, 118.61, 117.24 (d, J = 31.3 Hz), 113.78, 30.67. HRMS m/z (ESI) calcd for $C_{16}H_{11}N_2F_6$ $[M + H]^+$: 345.0821, found: 345.0839.

4g: ^{1}H NMR (400 MHz, DMSO-d_6) δ 11.96 (s, 1H), 8.52 (d, J = 2.2 Hz, 1H), 8.24 (d, J = 2.1 Hz, 1H), 7.51 (d, J = 2.2 Hz, 1H), 7.42–7.28 (m, 4H), 7.19 (t, J = 7.9 Hz, 1H), 7.03–6.94 (m, 1H),

6.89 (d, $J = 7.6$ Hz, 1H), 6.83 (s, 1H), 5.05 (s, 2H), 4.07 (s, 2H). ^{13}C NMR (101 MHz, DMSO-d_6) δ 158.88, 150.37, 143.05, 139.56, 137.56, 129.83, 128.80, 128.08, 126.81, 124.76, 121.40, 118.71, 117.09 (q, J = 31.3 Hz), 115.62, 114.56, 112.63, 69.54, 31.02. HRMS m/z (ESI) calcd for $C_{22}H_{18}N_2OF_3$ $[M + H]^+$: 383.1366, found: 383.1354.

4h: ^{1}H NMR (400 MHz, DMSO-d_6) δ 11.96 (s, 1H), 8.52 (d, $J =$ 2.1 Hz, 1H), 8.29 (d, $J = 2.2$ Hz, 1H), 7.53 (d, $J = 2.3$ Hz, 1H), 6.49 (d, $J = 2.3$ Hz, 2H), 6.31 (t, $J = 2.3$ Hz, 1H), 4.03 (s, 2H), 3.69 (s, 6H). ^{13}C NMR (101 MHz, DMSO-d_6) δ 160.90, 150.35, 143.78, 139.56 (d, $J = 4.1$ Hz), 126.79, 124.87, 124.83, 118.70, 116.92 (q, J = 31.5 Hz), 114.52, 107.12, 98.11, 55.50, 31.27. HRMS m/z (ESI) calcd for $C_{17}H_{16}N_2O_2F_3$ $[M + H]^+$: 337.1158, found: 337.1147.

4i: ^{1}H NMR (400 MHz, DMSO-d_6) δ 12.05 (s, 1H), 8.54 (d, $J =$ 2.1 Hz, 1H), 8.34 (d, $J = 2.1$ Hz, 1H), 7.51 (d, $J = 2.3$ Hz, 1H), 7.23 (td, $J = 9.2$, 4.7 Hz, 2H), 7.08 (m, $J = 12.2$, 8.1, 3.6 Hz, 1H), 4.13 (s, 2H). ^{13}C NMR (101 MHz, DMSO-d_6) δ 159.76, 158.11, 157.37 (d, $J = 2.1$ Hz), 155.74, 150.21, 139.74, 130.30 (dd, $J = 18.6$, 7.8 Hz), 127.19, 124.67, 118.46, 114.99, 114.84, 112.55, 49.06, 24.23. HRMS m/z (ESI) calcd for $C_{15}H_{10}N_2F_5$ $[M + H]^+$: 313.0759, found: 313.0752.

4j: ^{1}H NMR (400 MHz, DMSO-d_6) δ 12.06 (s, 1H), 8.54 (d, $J =$ 2.1 Hz, 1H), 8.36 (d, $J = 2.1$ Hz, 1H), 7.86 (s, 1H), 7.61 (dd, $J =$ 6.8, 1.9 Hz, 3H), 4.22 (s, 2H). ^{13}C NMR (101 MHz, DMSO-d_6) δ 150.33, 141.83, 139.80, 134.58, 132.06, 128.60, 128.13, 127.25, 127.04, 124.85, 122.02, 118.49, 117.29 (q, $J = 31.7$ Hz), 113.62, 29.92. HRMS m/z (ESI) calcd for $C_{16}H_{10}N_2F_6Cl$ $[M + H]^+$: 379.0430, found: 379.0435.

4k: ^{1}H NMR (400 MHz, DMSO-d_6) δ 12.01 (s, 1H), 8.52 (d, $J =$ 2.1 Hz, 1H), 8.31 (d, $J = 2.1$ Hz, 1H), 7.55 (d, $J = 2.4$ Hz, 1H), 7.38 (d, $J = 1.8$ Hz, 1H), 7.30 (d, $J = 8.3$ Hz, 1H), 7.18 (dd, $J = 8.2$, 1.7 Hz, 1H), 4.13 (s, 2H). ^{13}C NMR (101 MHz, DMSO-d_6) δ 150.31, 143.24, 141.48, 139.70, 139.68 (d, $J = 4.1$ Hz), 138.55, 131.61, 126.98, 124.77 (d, $J = 4.0$ Hz), 124.53, 118.51, 117.22 (q, $J = 31.7$ Hz), 114.37, 110.63, 110.17, 30.60. HRMS m/z (ESI) calcd for $C_{16}H_{10}N_2O_2F_5$ $[M + H]^+$: 357.0657, found: 357.0675.

4l: ^{1}H NMR (400 MHz, DMSO-d_6) δ 12.02 (s, 1H), 8.53 (d, $J =$ 2.1 Hz, 1H), 8.30 (d, $J = 2.1$ Hz, 1H), 7.72 (s, 1H), 7.68–7.57 (m, 2H), 7.57–7.46 (m, 2H), 4.23 (s, 2H). ^{13}C NMR (101 MHz, DMSO-d_6) δ 169.35, 164.01, 151.06, 150.37, 148.37, 139.81, 139.60, 138.52, 126.86, 125.20, 124.77 (d, $J = 4.4$ Hz), 119.08, 117.11 (d, J = 31.6 Hz), 114.90, 110.52, 31.03, 14.52. HRMS m/z (ESI) calcd for $C_{17}H_{13}N_3OF_3$ $[M + H]^+$: 332.1005, found: 332.1001.

2.2. Biological

2.2.1 Materials. The Annexin V–FITC Apoptosis Detection Kit was purchased from KeyGen Biotech (Nanjing, China). Dimethyl sulfoxide (DMSO) and 3-(4,5-dimethylthiazol-2-yl)-2,5-diphenyltetrazoliumbromide (MTT), 2-(6-amino-3-imino-3*H*-xanthen-9-yl)benzoic acid methyl ester (Rh123) and 2′,7′-dichlor-odihydrofluorescein diacetate (DCFH-DA) were purchased from Sigma Chemical Co. (St Louis, MO, USA). Hoechst 33358 and 0.5% crystal violet were bought from Beyotime (Beijing, China). The primary antibodies against TIMP2, matrix metalloproteinase9 (MMP9), cleaved caspase-3, Bcl2 were obtained from Cell Signaling Technology (Beverly, MA, USA). β-Actin was purchased from ZSJQ-BIO Co. (Beijing, China).

2.2.2 Cell lines and cell culture. The 4T1 were purchased from the American Type Culture Collection (Rockville, MD, USA). All cells were propagated in DMEM media containing 10% heat-inactivated fetal bovine serum (FBS, Hyclone, Logan, UT, USA) and 1% antibiotics (penicillin and streptomycin) in 5% CO_2 at 37 °C.

2.2.3 Cell viability assay. The cell viability of **4h**-treated 4T1 cells was assessed by MTT assay. Briefly, exponentially growing cells (2–6 × 10^3 cells per well) were seeded in 96-well plates and incubated for 24 h. Then the cells were treated with different concentrations of **4h** (0, 3.3, 10, 30 μM). After treatment for 24 h, 48 h and 72 h, respectively, 20 μL of 5 mg mL^{-1} MTT was added to each well and incubated for an additional 2–4 h at 37 °C. The medium was subsequently removed, and the purple-colored precipitates of formazan by the living cells were dissolved in 150 μL of DMSO. The color absorbance was recorded at 570 nm using a Spectra MAX M5 microplate spectrophotometer (Molecular Devices, Sunnyvale, CA, USA). The data presented are representative of two independent experiments.

2.2.4 Colony formation assay.[27] In brief, cells were seeded at a specified number (400–800 cells per well) in 6-well plates and treated with various concentrations of **4h** (0–30 μM) after 24 h incubation. The fresh medium with or without **4h** was changed every three days. After treatment for 12 days, the cells were washed with cold PBS, the colonies were fixed with methanol and stained with a 0.5% crystal violet solution for 15 min, and the colonies (<50 cells) were counted under a microscope.

2.2.5 Morphological analysis by Hoechst staining. To investigate whether the **4h** induced inhibition in cell viability was attributable to apoptosis, we stained the 4T1 cells with Hoechst 33258 dye. In brief, 4T1 cells (1–2 × 10^5 cells per well) were seeded onto an 18 mm cover glass in a 6-well plate for 24 h. After incubating with different concentrations for 48 h, the cells were washed with cold phosphate-buffered saline (PBS) and fixed in 4% paraformaldehyde for 15 min. The cells were stained with Hoechst 33258 solution (5 μg mL^{-1}). Then, the nuclear morphology of apoptotic cells was observed by fluorescence microscopy (Leica DM4000B, Leica, Wetzlar, Germany).

2.2.6 Apoptotic assay and flow cytometry.[27] To further confirm the apoptosis-inducing effects of **4h**, we subsequently estimated the number of apoptotic cells by flow cytometry (FCM). Briefly, 4T1 cells (1–2 × 10^5 cells per well) were seeded in six-well plates for 24 h. After treatment with various concentrations of **4h** for 24 h, the cells were harvested and washed with cold PBS twice. The apoptosis levels were examined using an Annexin V–FITC/PI detection kit by FCM. The data were analyzed with FlowJo software.

2.2.7 Western blot analysis.[28] Briefly, 4T1 cells were treated with **4h** in different concentration for 24 h, then cells were washed with cold PBS for two times and lysed in RIPA buffer. The protein concentrations were examined using the Lowry method and equalized before loading. Equal amounts of protein from each sample were separated on SDS-PAGE gel and transferred onto polyvinylidene fluoride (PVDF) membranes

(Amersham Bioscience, Piscataway, NJ). Then, the membranes were blocked for 1 h at 37 °C and incubated with specific primary antibodies overnight at 4 °C. After incubation with the relevant secondary antibodies for 1 h, the reactive bands were identified using an enhanced chemiluminescence kit (Amersham). Then, the images were analyzed using the Image J computer software (National Institute of Health, Bethesda, MD, USA).

2.2.8 Boyden chamber migration and invasion assay.[29] A total of 1×10^5 cells in 100 μL serum-free medium were added to the upper chamber, and 600 μL of medium containing 10% FBS was added at the bottom. Different concentrations of **4h** were added to both chambers. Cells were allowed to migrate for 24 h. Non-migrated cells in the upper chamber were discarded using a cotton swab. The migrated cells were fixed in methanol and stained with 0.5% crystal violet for 20 min. Migrated cells in six randomly selected fields were counted and photographed under a light microscope. The invasion assay was performed according to previous studies. In brief, the upper surface of the transwell membrane was coated with serum-free medium diluted Matrigel (1 : 5, 60 μL per well, BD Biosciences). After Matrigel polymerization, the lower compartment of the chambers was filled with 600 μL medium with 10% FBS and 5×10^4 cells in 100 μL serum-free medium were placed in the upper part of each transwell and treated with different concentrations of **4h**. After incubation for 24 h, cells on the upper side of the filter were removed. Cells located on the underside of the filter were fixed with methanol and stained with 0.5% crystal violet. Next, migrated cells were counted and photographed under a light microscope. The results were expressed as the percentage inhibition rate of migration compared with the untreated group.

2.2.9 Calculation of ligand efficiency. The calculation of the binding energy of the ligand per atom, or 'ligand efficiency' (ΔLE) could be calculated by converting the K_d into the free energy of binding [eqn (1)] at 300 K and dividing by the number of 'heavy' (non-hydrogen atoms) atoms [eqn (2)].[30]

Free energy of ligand binding:

$$\Delta G = -RT \ln K_d \quad (1)$$

Binding energy per atom (ligand efficiency):

$$\Delta LE = \Delta G/n \text{ (non-hydrogen atoms)} \quad (2)$$

The K_d value was replaced by IC_{50}.

Conflicts of interest

There are no conflicts to declare.

Acknowledgements

This work was supported by Post-Doctor Research Project, West China Hospital, Sichuan University, China (No. 2018HXBH009) and the Fundamental Research Funds for the Central Universities (No. 2020SCU12020, the Postdoctoral Foundation of Sichuan University).

Notes and references

1 M. Kostas, E. M. Haugsten, Y. Zhen, V. Sorensen, P. Szybowska, E. Fiorito, S. Lorenz, N. Jones, G. A. de Souza, A. Wiedlocha and J. Wesche, *Mol. Cell. Proteomics*, 2018, **17**, 850–870.
2 M. Wei, X. Peng, L. Xing, Y. Dai, R. Huang, M. Geng, A. Zhang, J. Ai and Z. Song, *Eur. J. Med. Chem.*, 2018, **154**, 9–28.
3 Y. K. Chae, K. Ranganath, P. S. Hammerman, C. Vaklavas, N. Mohindra, A. Kalyan, M. Matsangou, R. Costa, B. Carneiro, V. M. Villaflor, M. Cristofanilli and F. J. Giles, *Oncotarget*, 2017, **8**, 16052–16074.
4 G. C. Ghedini, R. Ronca, M. Presta and A. Giacomini, *Expert Rev. Anticancer Ther.*, 2018, **18**, 861–872.
5 A. De Luca, R. Esposito Abate, A. M. Rachiglio, M. R. Maiello, C. Esposito, C. Schettino, F. Izzo, G. Nasti and N. Normanno, *Int. J. Mol. Sci.*, 2020, **21**(18), 6856.
6 R. Porta, R. Borea, A. Coelho, S. Khan, A. Araujo, P. Reclusa, T. Franchina, N. Van Der Steen, P. Van Dam, J. Ferri, R. Sirera, A. Naing, D. Hong and C. Rolfo, *Crit. Rev. Oncol. Hematol.*, 2017, **113**, 256–267.
7 F. T. Liu, N. G. Li, Y. M. Zhang, W. C. Xie, S. P. Yang, T. Lu and Z. H. Shi, *Eur. J. Med. Chem.*, 2020, **186**, 111884.
8 M. Katoh and H. Nakagama, *Med. Res. Rev.*, 2014, **34**, 280–300.
9 A. Giacomini, P. Chiodelli, S. Matarazzo, M. Rusnati, M. Presta and R. Ronca, *Pharmacol. Res.*, 2016, **107**, 172–185.
10 W. Yan, X. Wang, Y. Dai, B. Zhao, X. Yang, J. Fan, Y. Gao, F. Meng, Y. Wang, C. Luo, J. Ai, M. Geng and W. Duan, *J. Med. Chem.*, 2016, **59**, 6690–6708.
11 I. S. Babina and N. C. Turner, *Nat. Rev. Cancer*, 2017, **17**, 318–332.
12 L. Balek, I. Gudernova, I. Vesela, M. Hampl, V. Oralova, M. Kunova Bosakova, M. Varecha, P. Nemec, T. Hall, G. Abbadessa, N. Hatch, M. Buchtova and P. Krejci, *Bone*, 2017, **105**, 57–66.
13 Y. Wang, Y. Dai, X. Wu, F. Li, B. Liu, C. Li, Q. Liu, Y. Zhou, B. Wang, M. Zhu, R. Cui, X. Tan, Z. Xiong, J. Liu, M. Tan, Y. Xu, M. Geng, H. Jiang, H. Liu, J. Ai and M. Zheng, *J. Med. Chem.*, 2019, **62**, 7473–7488.
14 Y. Zhou, C. Wu, G. Lu, Z. Hu, Q. Chen and X. Du, *J. Cancer*, 2020, **11**, 2000–2007.
15 P. R. Gavine, L. Mooney, E. Kilgour, A. P. Thomas, K. Al-Kadhimi, S. Beck, C. Rooney, T. Coleman, D. Baker, M. J. Mellor, A. N. Brooks and T. Klinowska, *Cancer Res.*, 2012, **72**, 2045–2056.
16 T. Nishina, S. Takahashi, R. Iwasawa, H. Noguchi, M. Aoki and T. Doi, *Invest. New Drugs*, 2018, **36**, 424–434.
17 Y. Nakanishi, N. Akiyama, T. Tsukaguchi, T. Fujii, K. Sakata, H. Sase, T. Isobe, K. Morikami, H. Shindoh, T. Mio, H. Ebiike, N. Taka, Y. Aoki and N. Ishii, *Mol. Cancer Ther.*, 2014, **13**, 2547–2558.

18 V. Guagnano, P. Furet, C. Spanka, V. Bordas, M. Le Douget, C. Stamm, J. Brueggen, M. R. Jensen, C. Schnell, H. Schmid, M. Wartmann, J. Berghausen, P. Drueckes, A. Zimmerlin, D. Bussiere, J. Murray and D. Graus Porta, *J. Med. Chem.*, 2011, **54**, 7066–7083.

19 G. Zhao, W. Y. Li, D. Chen, J. R. Henry, H. Y. Li, Z. Chen, M. Zia-Ebrahimi, L. Bloem, Y. Zhai, K. Huss, S. B. Peng and D. J. McCann, *Mol. Cancer Ther.*, 2011, **10**, 2200–2210.

20 P. C. C. Liu, H. Koblish, L. Wu, K. Bowman, S. Diamond, D. DiMatteo, Y. Zhang, M. Hansbury, M. Rupar, X. Wen, P. Collier, P. Feldman, R. Klabe, K. A. Burke, M. Soloviev, C. Gardiner, X. He, A. Volgina, M. Covington, B. Ruggeri, R. Wynn, T. C. Burn, P. Scherle, S. Yeleswaram, W. Yao, R. Huber and G. Hollis, *PLoS One*, 2020, **15**, e0231877.

21 The website of Erdafitinib approved by FDA, https://www.fda.gov/drugs/new-drugs-fda-cders-new-molecular-entities-and-new-therapeutic-biological-products/novel-drug-approvals-2019.

22 The website of Pemigatinib approved by FDA, https://www.fda.gov/drugs/new-drugs-fda-cders-new-molecular-entities-and-new-therapeutic-biological-products/novel-drug-approvals-2020.

23 J. Tsai, J. T. Lee, W. Wang, J. Zhang, H. Cho, S. Mamo, R. Bremer, S. Gillette, J. Kong, N. K. Haass, K. Sproesser, L. Li, K. S. Smalley, D. Fong, Y. L. Zhu, A. Marimuthu, H. Nguyen, B. Lam, J. Liu, I. Cheung, J. Rice, Y. Suzuki, C. Luu, C. Settachatgul, R. Shellooe, J. Cantwell, S. H. Kim, J. Schlessinger, K. Y. Zhang, B. L. West, B. Powell, G. Habets, C. Zhang, P. N. Ibrahim, P. Hirth, D. R. Artis, M. Herlyn and G. Bollag, *Proc. Natl. Acad. Sci. U. S. A.*, 2008, **105**, 3041–3046.

24 Q. Jin, D. Zhang, M. Gao, C. Jiang and J. Zhang, *Bioorg. Med. Chem.*, 2021, **29**, 115862.

25 L. Crocetti, M. P. Giovannoni, I. A. Schepetkin, M. T. Quinn, A. I. Khlebnikov, N. Cantini, G. Guerrini, A. Iacovone, E. Teodori and C. Vergelli, *Bioorg. Med. Chem.*, 2018, **26**, 5583–5595.

26 S. Narva, S. Chitti, B. R. Bala, M. Alvala, N. Jain and V. G. Kondapalli, *Eur. J. Med. Chem.*, 2016, **114**, 220–231.

27 T. Ye, X. Wei, T. Yin, Y. Xia, D. Li, B. Shao, X. Song, S. He, M. Luo, X. Gao, Z. He, C. Luo, Y. Xiong, N. Wang, J. Zeng, L. Zhao, G. Shen, Y. Xie, L. Yu and Y. Wei, *Breast Cancer Res. Treat.*, 2014, **143**, 435–446.

28 Y. Li, C. Gan, Y. Zhang, Y. Yu, C. Fan, Y. Deng, Q. Zhang, X. Yu, Y. Zhang, L. Wang, F. He, Y. Xie, T. Ye and W. Yin, *Front. Pharmacol.*, 2019, **10**, 1195.

29 C. Gan, Y. Li, Y. Yu, X. Yu, H. Liu, Q. Zhang, W. Yin, L. Yu and T. Ye, *Bioorg. Med. Chem.*, 2019, **27**, 115089.

30 A. L. Hopkins, C. R. Groom and A. Alex, *Drug Discovery Today*, 2004, **9**, 430–431.